

CHARACTERIZATION OF NEURAL INTERACTION DURING LEARNING AND ADAPTATION FROM SPIKE-TRAIN DATA

LIQIANG ZHU

Department of Electrical Engineering, Arizona State University
Tempe, AZ 85287

YING-CHENG LAI

Department of Mathematics and Statistics, Department of Electrical Engineering
Arizona State University, Tempe, AZ 85287

FRANK C. HOPPENSTEADT

Courant Institute, New York University
New York, NY 10012

JIPING HE

Department of Bioengineering, Arizona State University
Tempe, AZ 85281

(Communicated by Jianhong Wu)

ABSTRACT. A basic task in understanding the neural mechanism of learning and adaptation is to detect and characterize neural interactions and their changes in response to new experiences. Recent experimental work has indicated that neural interactions in the primary motor cortex of the monkey brain tend to change their preferred directions during adaptation to an external force field. To quantify such changes, it is necessary to develop computational methodology for data analysis. Given that typical experimental data consist of spike trains recorded from individual neurons, probing the strength of neural interactions and their changes is extremely challenging. We recently reported in a brief communication [Zhu et al., *Neural Computations* **15**, 2359 (2003)] a general procedure to detect and quantify the causal interactions among neurons, which is based on the method of directed transfer function derived from a class of multivariate, linear stochastic models. The procedure was applied to spike trains from neurons in the primary motor cortex of the monkey brain during adaptation, where monkeys were trained to learn a new skill by moving their arms to reach a target under external perturbations. Our computation and analysis indicated that the adaptation tends to alter the connection topology of the underlying neural network, yet the average interaction strength in the network is approximately conserved before and after the adaptation. The present paper gives a detailed account of this procedure and its applicability to spike-train data in terms of the hypotheses, theory, computational methods, control test, and extensive analysis of experimental data.

2000 *Mathematics Subject Classification.* 62H20, 62P10.

Key words and phrases. neural learning, neural interaction, primary motor cortex, multivariate analysis, directed transfer function, Granger causality.

1. Introduction. Learning is among the most important functions of the brain. As the brain acquires a new skill and adapts to new circumstances, structural and dynamical changes may occur in the corresponding parts of the brain. Depending on the nature of the new knowledge or skill, the group of neurons responsible for the learning can vary. Broadly speaking, for a given task, specific networks (or subnetworks) of neurons are responsible for learning and adaptation. Understanding how the network characteristics, such as the connecting architecture and coupling strength among neurons, change in response to learning and adaptation is of paramount importance and interest. Among the many existing studies on neural mechanisms for learning and adaptation, motor learning is of primary interest because of the relative ease in accessibility to controlled experimental studies. A wealth of evidence suggests that motor learning involves many areas of the brain, among them the cerebellum and the basal ganglia [1, 2] which are traditionally believed to be limited to motor control at the subcortical level, the motor cortex [3, 4] which mainly plans and controls movement, the sensory cortex, and other association areas [5].

In this paper, we focus on the primary motor cortex (M1), believed to be responsible for voluntary movements. M1 contains several subdivisions, corresponding to movements of major body parts such as arms, legs, or the face. Each subdivision has an internal network with the capabilities to respond to, to learn, and to control a rich variety of functions. Recent studies on human and nonhuman primates [6, 7, 8, 9] demonstrate that M1 is plastic, indicating the dynamic and adaptive nature of the area. At the level of single neurons, a recent work [4] explored changes in *individual* neurons in response to motions in preferred direction, concluding that two classes of neurons in M1 coexist and interact with each other to provide the functions of motor learning and operations. In addition, these neurons also carry the memory necessary for learning and controlling the movement. Neurons in M1 are apparently connected in a sophisticated manner. Because of the ubiquitous presence of neural plasticity, it is reasonable to hypothesize that neural interactions are also responsible for learning and organizing specific movements. Yet to our knowledge, little has been done to explore the interactions among neurons in M1 and how they change to learn a specific type of movement and to adapt to new conditions. The aim of this paper is to characterize, quantitatively, interactions among M1 neurons and how they change in response to movement perturbations in a series of controlled experiments with monkeys.

Our analysis is based on constructing a class of linear stochastic models, namely the multivariate autoregressive (MVAR) models, from recordings of a group of neurons in M1 during learning and adaptation, and on computing the associated directed transfer functions (DTFs) in the frequency domain. The reasons we choose to work with linear, stochastic models are the following. Traditionally, nonparametric methods based on correlation measurements and spectral-coherence analysis are popular for probing the neuronal interactions [10, 11, 12]. These methods deal with a pair of recordings from different neurons over a relatively long period, and they pose several difficulties. First, focusing on the long-term behavior of two neurons without taking into account influences from other neurons will inevitably classify any detectable interaction as direct, while typically indirect interactions can take place between any pair of neurons. Second, the methods require stationarity, which cannot hold over a long period of time in typical experiments. Third, nonparametric methods usually yield no information about the direction of the interaction between

the pair of neurons, as the spectral coherence computed from correlation is independent of whether the coupling is forward or backward. Recently, spike pattern classification methods [13, 14, 15] were proposed to measure interactions among neurons from spike trains. These methods are based on evaluating the statistical significance of spike patterns across channels and time. The patterns that occur more frequently than random coincidence are called unitary events [13, 14, 15]. The interactions among involved neurons are presented by the spike patterns. Although appealing, these methods are very sensitive to non-stationarity and changes in firing rate, making it difficult to distinguish results from statistical artifacts. The MVAR [16, 17, 18] and DTF methods [19, 20, 21, 22] that we will use are justified by the reasonable and practical assumption that neural recordings can be regarded as a result of an intrinsically stochastic process. These methods have proven to be powerful for analyzing multichannel neural recordings [19, 20, 21, 18, 22].

The neural recordings used in our construction of the linear MVAR model and subsequent computation of DTFs are spike trains from neurons in M1 of a monkey, which are typically short and sparse. It is necessary to preprocess the data so that the MVAR model can effectively approximate the stochastic process that generates the spike trains. We propose a method to achieve this by converting the spike trains into continuous-time signals of the instantaneous spiking rate. Then, by measuring the average coupling strength based on the concept of Granger causality [23] and DTFs, we can assess the changes in neural interactions in a *quantitative* manner. Our main findings are (1) learning and adaptation typically result in significant temporal changes in the interactions among neurons, (2) these changes occur both in the direction and the strength of coupling, (3) the average coupling strength over the network of neurons involved increases during the learning but returns to the original level after adaptation, which is naturally expected based on consideration of factors such as energy conservation, and (4) the connecting architecture of the network is typically altered after adaptation. A brief report on part of this work appeared recently [24].

Neural activities in the brain are undoubtedly nonlinear. Naturally, one might ask why we choose to focus on linear methods to address the learning and adaptation problem in M1. Like linear methods, nonlinear methods can be classified as nonparametric and parametric. A popular class of nonparametric method is nonlinear time-series analysis based on the assumption that the underlying dynamical system generating the time series is deterministic and therefore the corresponding phase space, the space in which all dynamical trajectories live, can be reconstructed by using a proper embedding method [25, 26, 27]. Two limitations, which at present appear to be fundamental, hamper the use of the nonlinear embedding method for neural data. They are noise and the intrinsic high-dimensionality of the underlying dynamical system that generates the neural activities, as the embedding method can yield meaningful information only for relatively noiseless data and for systems of low dimensionality [27]. For neural data that contain a large number of spikes, a method of constructing embedding by using interspike time intervals was proposed [28, 29, 30]. However, for the task we face, the neural recordings typically consist of trains that contain very few spikes, for which the interspike-interval embedding method is apparently not applicable. Mutual information is also widely used to measure the association between two spike trains. Use of the information measurement is motivated by the idea that the responsible parts of the nervous system, such as visual pathways, may be modeled as communication channels. Irrespective

of the validity of this idea, mutual information methods also face difficulties, such as the required large data sets that might be obtained from experiments. Parametric methods, on the other hand, utilize nonlinear modeling such as artificial neural networks and fuzzy-logic models to identify the underlying nonlinear system and to estimate the interactions among neurons, which is promising; however, the methods are largely empirical and generally more difficult to deal with than linear methods. For instance, in the artificial neural-network approach, the number of adjustable parameters can be enormously large. Our philosophy is that, given a set of neural data that are typically noisy and short, the linear method should be considered first, at least for the purpose of gaining insights. Often such an exploration can lead to meaningful results. Indeed, as we will demonstrate in this paper, by carefully preprocessing the input data and selecting model parameters, the MVAR/DTF-approach can yield a rich amount of information that can help us better understand the functional changes in the neural interactions during learning and adaptation. Application of nonlinear parametric models such as artificial neural networks to the problem addressed in this paper should, however, be investigated.

2. Material and methods.

2.1. Behavioral experiments and data collection. The experimental subject is a rhesus monkey trained to perform behavioral movements according to instructions. The Institutional Animal Care and Use Committee at Arizona State University approved the behavioral paradigm, surgical procedures, and general animal care. A typical experiment setting consists of eight targets with lightened push-buttons located at the vertices of a 13 cm cube, as shown in Figure 1. In the center of the cube is an additional target. Each trial begins with the illumination of the central target (center-on). The monkey is trained to push and hold the button on the central target until a randomly selected target at a vertex is illuminated, at which time the monkey is supposed to reach out to the new target. The time allowed for the monkey to accomplish the reach-out movement is 750 milliseconds. Typically, a monkey's reacting time (the time required for the monkey to release the central button and reach a vertex target) is about 200 milliseconds. A successful trial requires that the monkey reach the vertex target and push the button in time less than 600 milliseconds.

To assess the neural behavior in M1, four 16-channel arrays of microelectrodes are chronically implanted in the pre- and post-central arm areas. Extracellular potentials are recorded on a 96 channel MAP (Plexon, Inc., Dallas, TX), allowing us to isolate up to four units on a single electrode on line, with waveform discrimination. A threshold crossing marks the occurrence of an action potential (spike), and spike times from all active channels are recorded in a data file along with the behavioral event times (for example, the center-release time), allowing us to separate the internal cognitive periods of the brain. In what follows, we will focus on neural recordings during the time period from target-on to center-release, during which M1 undergoes a planning process for voluntary movements.

To test the monkey's ability to learn and to adapt, at the behavioral level perturbations are applied to disturb the monkey's already well-trained reaching-out movement. To apply the perturbation, a string is attached to the monkey's wrist and a brief pulling force, lasting for 75 milliseconds is delivered through the string. Before the surgery, the monkey was first trained to perform unperturbed trials successfully, without the string attached. Then electrodes were implanted. After one

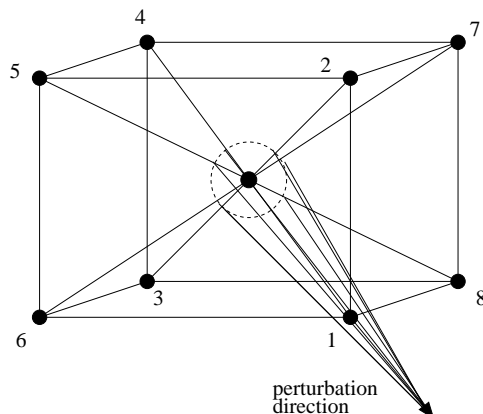


FIGURE 1. Targets and perturbation force field. The eight targets are located at the vertices of a 13 cm cube.

week of post-surgical recovery, the monkey was attached to the string during all experiments, no matter whether the perturbation was applied. The experiments began with four-week unperturbed trials. The average trajectory on the last day of unperturbed trials is shown in Figure 2 (the trajectory with ‘0’). From day one, the perturbation force was applied. At the beginning, the perturbation force tended to significantly displace the monkey’s arm motion from its normal, unperturbed trajectory. After about one week, the monkey could compensate for the perturbation in a fairly predictable way [31], which can be seen by comparing the trajectories on days 1 and 8 in Figure 2(a).

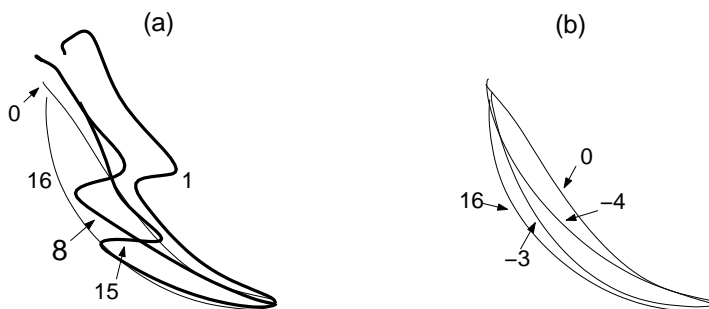


FIGURE 2. The hand trajectories toward target 4. The numbers indicate the experiment date; for example, ‘1’ indicates the first day of perturbed trials. Each trajectory shown here is averaged over all the trials during one day. The thick curves correspond to perturbed trials, and the thin curves to unperturbed trials.

2.2. MVAR model and its validity. The analysis method is based on MVAR modeling and the concept of Granger causality. Suppose multichannel time series $\mathbf{X}(n) = [x_1(n), x_2(n), \dots, x_M(n)]^T$ are generated from a stochastic system or a deterministic system of high dimensionality under the influence of strong noise. The current state is determined by the linear combination of K previous states

and uncorrelated white noise $\mathbf{N}(n) = [n_1(n), n_2(n), \dots, n_M(n)]^T$, if the time span between the previous and current state is not too large. In MVAR modeling, $\mathbf{X}(n)$ is written as

$$\mathbf{X}(n) = \sum_{k=1}^K \mathbf{A}(l) \cdot \mathbf{X}(n-l) + \mathbf{N}(n), \quad (1)$$

where $\mathbf{A}(l)$'s ($l = 1, \dots, K$) are $M \times M$ coefficient matrices, K is the model order, and the noisy vector $\mathbf{N}(n)$ characterizes the modeling error.

For a finite data set, increasing K , or the complexity of the model, can always reduce the modeling error $N(n)$ in general. However, if K is too large, overfitting may occur for a finite data set. A common approach to avoid overfitting is to use some information measure, which in general is a loss function with the complexity penalty. That is, a penalty is applied if K is too large (the model is too complex). The value of K at which the information measure achieves a minimum is regarded as optimal. Here, we use the Akaike's final-prediction-error (FPE) measure [32] to find optimal value of K , which is defined as

$$\text{FPE} = N_x \ln E + N_x \ln \frac{N_x + N_A}{N_x - N_A}, \quad (2)$$

where N_x is the number of data samples, N_A is the number of model parameters ($N_A < N_x$), and $E \equiv (1/N_x) \sum_{n=1}^{N_x} N^2(n)$ is the average of error squared. The second term in Equation (2) is the complexity penalty, which tends to zero as N_x approaches infinity.

Equation (1) is a linear model, and hence it can represent exactly noiseless linear systems for a suitable choice of K . In principle, it can also be used to model nonlinear or chaotic systems if the coefficient matrices are not constant but depend on the state of the system and K is sufficiently large (typically K should be at least twice as large as than the dimension of the dynamical invariant set in the phase space that generates the observed time series [25, 26]). Dealing with such a situation is difficult. While the underlying dynamical system generating the observed neural activities is undoubtedly nonlinear [33, 34, 35], its dimensionality may be so high that, effectively, it cannot be distinguished from a linear stochastic process [36]. Our central hypothesis then is that, practically, the neural dynamics of the brain can be described by linear stochastic models such as Equation (1).

Another issue concerns the stationarity of the stochastic process. Notice that the MVAR model defined by Equation (1) is time invariant, which requires that the time series $\mathbf{X}(n)$ be stationary. Strictly speaking, a stochastic process is stationary if its statistical properties are invariant in time. In practice, stationarity in a wide sense is convenient. A stochastic process $X(n)$ is called wide-sense stationary (WSS) if its mean is constant and its autocorrelation depends only on $c = n_1 - n_2$:

$$\begin{aligned} E\{X(n)\} &= \mu, \\ E\{X(n+c)X(n)\} &= R(c). \end{aligned} \quad (3)$$

Two stochastic processes $X_1(n)$ and $X_2(n)$ are called jointly WSS if each is WSS and their cross-correlation depends on c only:

$$E\{X_1(n+c)X_2(n)\} = R_{X_1X_2}(c). \quad (4)$$

Thus, in the wide sense so described, it is suitable to model multichannel time series $\mathbf{X}(n)$ by Equation (1) if each channel is WSS and all channels are jointly WSS. However, in our experiment, during the reaching-out movement, the monkey's brain

performs a cognitive task, which may be sensitively influenced by various disturbances from the environment. The state of the brain may thus change rapidly in time, which in turn, results in changes in the firing rate, in the pattern of the neurons, and likely in the functional interactions between neurons as well. In reality, neural recordings are thus nonstationary. While the stationarity of recording from individual channels may be improved by making $E\{x(n)\}$ and $R(0)$ constant (that is, by subtracting mean and dividing by standard deviation for each point in the time series), computationally it is hard to improve the joint stationarity. Nonetheless, if the interactions among neurons in different regions, reflected in the recordings from different channels, are approximately invariant or slowly varying over a short time period on which the analysis is focused, the cross-correlation functions can be assumed to be approximately time-invariant. This is the reason we focus on the short period from target-on to center-release in our analysis. The underlying assumption is that over this time interval, the interactions among neurons change little with time.

2.3. Directed transfer function. In Equation (1), the signal from the j th channel at time n can be explicitly written in terms of the signals from all other channels at a set of earlier times as

$$x_j(n) = \sum_{l=1}^K A_{j1}(l)x_1(n-l) + \dots + \sum_{l=1}^K A_{jM}(l)x_M(n-l) + n_j(n). \quad (5)$$

In Equation (5), if the presence of the past signal from the i th channel can help reduce the modeling error $n_j(n)$ in the signal $x_j(n)$ of the j th channel, the i th channel is said to be *causal* to the j th channel [19]. That is, if $A_{ji}(l)$ ($l = 1, \dots, K$) are not zero, statistically there is a causal influence from channel i to channel j . Performing Fourier transform of Equation (1) yields

$$\mathbf{X}(f) = \mathbf{A}^{-1}(f) \cdot \mathbf{N}(f) \equiv \mathbf{H}(f) \cdot \mathbf{N}(f), \quad (6)$$

where $\mathbf{X}(f)$ and $\mathbf{N}(f)$ are the Fourier transforms of $\mathbf{X}(n)$ and $\mathbf{N}(n)$, respectively, and the matrix $\mathbf{A}(f)$ is given by

$$\mathbf{A}(f) = -\sum_{l=0}^K \mathbf{A}(l)e^{-j2\pi fl},$$

with $\mathbf{A}(l=0) = -\mathbf{I}$ (\mathbf{I} being identity matrix). The inverse matrix $\mathbf{A}^{-1}(f) \equiv \mathbf{H}(f)$ is the transfer-function matrix of the system in the frequency domain. Kaminski and Blinowska [19] define the DTF from the i th channel to the j th channel as

$$\text{DTF}(f)_{ji} = \frac{|H_{ji}(f)|^2}{\sum_{m=1}^M (|H_{jm}(f)|^2)}. \quad (7)$$

To demonstrate the power of DTFs in characterizing the mutual interactions or couplings among neurons, we consider an artificial network consisting of five neurons, as shown in Figure 3. The details of the computational model for the network will be described in Section 3. Here we just illustrate the behavior of the computed DTFs. The DTFs for a pair of neurons (2 and 3 in Figure 3), are shown in Figure 4. In the assumed network configuration, there is a unidirectional interaction between the two neurons in the sense that there is an influence from neuron 2 to neuron 3, but not the other way around. This feature is correctly reflected in the DTFs, as shown in Figures. 4(a) and 4(b), where we see that the transfer function $\text{DTF}_{32}(f)$

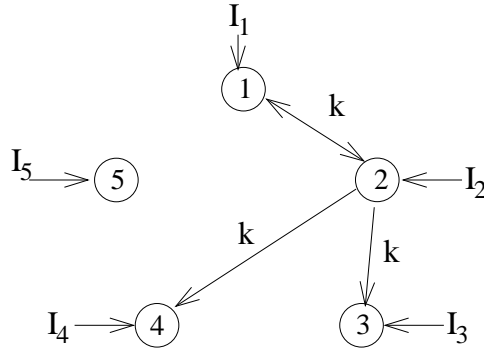


FIGURE 3. An example illustrating the use of DTFs. There are five neurons: four connected and one isolated. All neurons are driven by independent external stimuli- independent bandpass noise in the simulation. The mutual interactions among the neurons are explicitly reflected by the values of the DTFs, as we have demonstrated using a numerical model (see Section 3 for details).

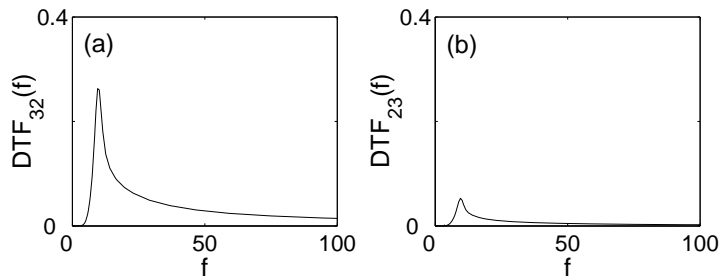


FIGURE 4. Directed transfer functions between neuron 2 and 3 shown in Figure 3.

has a pronounced peak around $f = 10Hz$ (indicating a significant influence from neuron 2 to neuron 3), while the value of the function $DTF_{23}(f)$ is close to zero for almost all frequencies, signifying the lack of a substantial influence from neuron 3 to neuron 2, as should be.

From Figures. 4(a) and 4(b), we see that a convenient quantity to characterize the interactions among neurons is

$$\int_0^{\infty} DTF(f)df,$$

which is the total area under the transfer function and can be regarded as proportional to the “energy” transfer, or the *direct* coupling, from one neuron to another. Motivated by this consideration, we define the direct coupling strength from neuron i to neuron j as

$$C_{ji} = \int_0^{\infty} DTF_{ji}(f)df. \quad (8)$$

Equivalently, one can make use of the coefficient matrices $\mathbf{A}(l)$ in the time domain to define the coupling strength [22], as follows:

$$C_{ji} = \frac{\sum_{l=1}^K A_{ji}^2(l)}{\sum_{j,i=1}^M \sum_{l=1}^K A_{ji}^2(l)}, \quad (9)$$

where $0 \leq C_{ji} \leq 1$.

The above definition of the coupling strength C_{ji} is meaningful only in the statistical sense. To test whether the computed values of the coupling strengths are statistically significant, it is necessary to conduct a null-hypothesis test. In this regard, the surrogate data method [37, 22] is convenient. For a set of given time series, its surrogate is generated by random shuffling of these recorded signals among themselves so that any functional interactions among them are destroyed while the energy of the original signals is maintained. Then the distribution of the coupling-strength measurement, $F(x) = \text{Probability}(C > x)$, can be empirically obtained by using a large number of independently shuffled surrogate data sets. For a given significance level α ($= 0.05$ used in this study), the causal influence from channel i to j is said to be significant if $F(C_{ji}) < \alpha$. The relative coupling strength can be evaluated as $C_{ji} - C_{ji}^s$, where C_{ji}^s is the averaged coupling strength from channel i to channel j based on the DTFs computed from the surrogate signals.

2.4. Dealing with short, sparse spike trains. The method described in Sections 2.2 and 2.3 to detect the causal interactions among neurons by using multichannel, simultaneous observations applies directly to continuous-time signals. If the recorded signals are long and relatively stationary, it is straightforward to apply MVAR modeling and consequently to measure the coupling strength. For nonstationary signals, it may be necessary to preprocess the data to reduce the influence of nonstationarity, such as removing the time-varying average from the data, dividing it into a set of short but relatively stationary segments, or both. In situations where only short time series are available, MVAR modeling requires an ensemble of such data sets. It is generally more desirable to have one MVAR model to fit all available data sets than to have one model for each data set and then to average the model results, as the MVAR model obtained from a short time series may be unstable in the sense that the eigenvalues of the transfer matrix may fall outside the unit circle in the complex plane.

Our neural recordings are even worse than merely short, because they are not continuous-time time series but spike trains, which can be regarded as coming from a point process. That is, the recorded information is a set of ordered times at which spikes occur, as follows:

$$t_0 < t_1 < t_2 < \dots < t_n < \dots$$

To apply a multivariate time-series analysis, one must convert the sequence of times into a continuous-time waveform [38]. A standard technique is to construct

$$x(t) = \sum_n \delta(t - t_n) \quad (10)$$

and then pass $x(t)$ through a low-pass filter, or to convolve $x(t)$ with a kernel function to remove high-frequency components [20, 22], generating a continuous time series more suitable for MVAR modeling and also capable of yielding the phase information of the spike train. Such a preprocessing is useful if the spike train contains a large number of spikes and the recordings are relatively stationary. We note

that for multichannel recordings, the relative phase, or the relative timing of spikes among different channels, is the only information from which neural interactions may be extracted. The relative timing is related to the temporal-coding hypothesis in neuroscience [39].

The neural data from our experiments contain only a sparse set of spikes, the number of which is typically so small that the aforementioned standard preprocessing method becomes unsuitable. Here we propose a general method to deal with short, sparse spike trains so that the MVAR modeling can be applied. The basic idea is to convert a spike train into time series of *instantaneous firing rate*. This is motivated by the two popular hypotheses in neural coding: rate modulation coding and temporal coding. Typically, the firing rate of a single neuron can be related to behavioral events, such as response to an external stimulus or a motor movement. Because of the sensitivity of the neural activity on small disturbances, even for the same movement and under the same external condition, the pattern of the instantaneous firing rate may change. While one may compute the mean discharge profile by averaging neural responses over many trials, comparison of these profiles from different neurons will yield little information about the neural interactions, because the averaging process destroys fine temporal correlation among the signals. Since large populations of neurons are involved simultaneously in any behavioral movements, the temporal structure of spike activity should influence the function of neural assemblies and thus provide coding information as well. That is, both rate and temporal information will be important for assessing the interaction among neurons. In a recent work [40], Riehle et al. demonstrated that synchronization of spiking activity (temporal coding) and modulation of discharge rates (rate coding) may represent two independent computational strategies used by the brain.

The *instantaneous* discharge rate in fact contains information about the temporal coding. As such, the rate profile and the original spike train code the same temporal firing behavior of the neuron. Consider, for example, integrate-and-fire neurons. If the firing threshold is known, the instantaneous firing rate can be converted into a spike train, and vice versa, without loss of information. In particular, the phase information is preserved. Fluctuations in the instantaneous firing rate reflect the irregularity in the occurrences of spikes, so a coherence measure between two instantaneous firing-rate time series can yield information about the causal interactions between the two neurons. Since the instantaneous rate profile can be regarded as a continuous-time signal, multivariate time-series analysis techniques can be applied readily.

Our procedure in constructing a continuous rate-function from a spike train consists of three steps, as shown in Figure 5. First, the instantaneous firing rate is approximated by the inverse of the interspike interval. To illustrate this, consider three successive spikes occurring at times t_{i-1} , t_i , and t_{i+1} , respectively. There are two interspike intervals: $\tau_{i-1} = t_i - t_{i-1}$ and $\tau_i = t_{i+1} - t_i$, giving rise to the following rate function:

$$r(t) = \begin{cases} 1/\tau_{i-1} & \text{for } t_{i-1} \leq t < t_i, \\ 1/\tau_i & \text{for } t_i \leq t < t_{i+1}. \end{cases} \quad (11)$$

Secondly, a small time interval δT is chosen to yield the instantaneous integrated rate

$$f^i(t) = \int_t^{t+\delta T} r(t)dt, \text{ for } t_{i-1} \leq t < t_{i+1}, \quad (12)$$

where δT is much smaller than the mean interspike interval T . For a train containing N spikes, $N - 2$ such functions $f^i(t)$ ($i = 2, \dots, N - 1$) can be computed. The third step is to smooth out these functions in time, yielding a continuous-time rate signal. The temporal property of the rate signal obtained this way lies somewhere between those of the mean rate profile and the original spike train, with δT as the parameter for adjusting the relative weights of the two. Although varying δT , insofar as it is smaller than T , will generally not affect the result, we find that, empirically, choosing δT to be a fraction of T (say $T/4$) is proper.

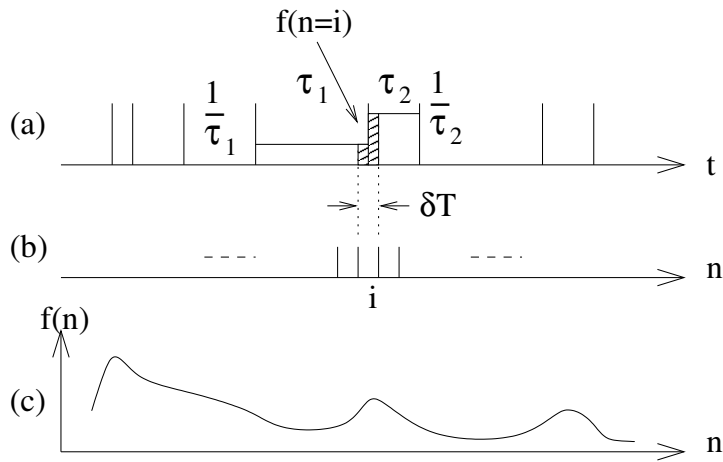


FIGURE 5. Construction of a continuous-time rate signal from a spike train. (a) Original spike train. The averaged firing rate during each interspike interval (e.g. τ_1) is taken to be the inverse of the interval (e.g. $1/\tau_1$). (b) Forming a time series with sampling period δT , where $f(n = i)$ is the area of shaded region in (a). (c) The resulting continuous-time rate signal, after low-pass filtering (FIR with cutoff frequency equal to 0.2 of the Nyquist frequency).

3. Results. In this section, we apply MVAR modeling and coupling-strength measurement to estimate the neural interactions from short, sparse spike trains. To gain confidence in the applicability of our method to realistic neural recordings, we first study a small artificial neural network consisting of five interacting, Hodgkin-Huxley type neurons, as shown in Figure 3. We then report results from monkey M1 neurons during learning and adaptation.

3.1. Benchmark testing using a model network of Hodgkin-Huxley type neurons. In this network, each neuron is modeled by the following set of ordinary

differential equations [41]:

$$\begin{aligned}
\frac{dV}{dt} &= -(17.81 + 47.58V + 33.8V^2)(V - 0.48) \\
&\quad - 26R(V + 0.95) + I - kg(V - E_{syn}), \\
\frac{dR}{dt} &= \frac{1}{5.6}[-R + 1.29V + 0.79 + 3.3(V + 0.38)^2], \\
\frac{df}{dt} &= \frac{1}{\tau_{syn}}[-f + Sgn(V_{pre} - \Omega)], \\
\frac{dg}{dt} &= \frac{1}{\tau_{syn}}(-g + f),
\end{aligned} \tag{13}$$

where $Sgn(x)$ is the sign function, V is membrane potential, R is the recovery variable, and f is an intermediate variable for synaptic potential g . The first two equations characterize the dynamics of the membrane potential, which are the simplified version of the Hodgkin-Huxley equations for mammalian cortical neurons. The last two equations govern the dynamics of the synaptic potential. All synapses in the network have the same coupling strength k , and E_{syn} is the synaptic equilibrium potential. In our simulation, we choose the synapses to be excitatory by setting $E_{syn} = 0$ and $k \geq 0$, although choosing inhibitory synapses by setting negative values for E_{syn} and k does not affect our results on detecting the interactions between the neurons. In Equation (13), τ_{syn} is the time constant of the synaptic potential, V_{pre} is the membrane potential of the presynaptic neuron, Ω is the threshold for postsynaptic conductance changes, and I is the sum of external stimuli, excluding the one from the presynaptic neuron. Independent low-pass filtered random noise is used to mimic external stimuli for different neurons. Typical waveforms of I are shown in Figure 6. Briefly, the membrane potential V_{pre} of the presynaptic neuron is coupled to that of the postsynaptic neuron V , through an excitatory or inhibitory synapse with time constant τ_{syn} .

We integrate Equation (13) using a standard routine (fourth order Runge-Kutta) with $k = 2$. Figure 7 shows the action potentials from the five neurons for one stimulus. On average, each neuron fires about 16 to 30 spikes during the period of one trial. While the data obtained from simulations are continuous-time signals, to mimic the situation in real experiments on monkeys, we convert them to spike trains by recording the time position of each spike and then using our procedure based on the instantaneous firing rate to reconvert the spike trains into continuous-time signals. We perform the same procedure for 100 independent trials. To improve the stationarity, the ensemble mean is subtracted and the data set is normalized by the standard deviation. An MVAR model is constructed from the resulting data. The FPE criterion gives the optimal model order of eight. Using the procedure in Equation (9), we obtain the coupling-strength matrix C . Similarly, we can obtain the matrix of a surrogate data set. For the null-hypothesis test, we repeat this process 100 times and obtain the empirical distribution of the coupling-strength measurement for each connection. A significance test gives the final estimation of the network coupling architecture, as shown in Figure 8. As expected, neuron 5 is isolated from the rest of the network, neurons 1 and 2 are bidirectionally coupled and there is no direct interaction between neurons 3 and 4, which are driven by neuron 2. The simulation indicates the presence of a small amount of coupling from neurons 4 to 2, which seems to contradict the original coupling configuration. However, considering the fact that this energy leakage occupies only a very small

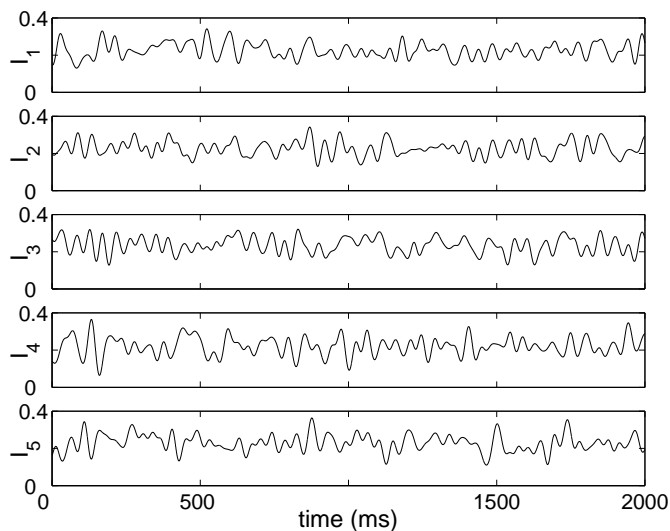


FIGURE 6. Typical waveforms of external stimuli or low-pass filtered independent noise used to drive the Hodgkin-Huxley neurons in our simulation.

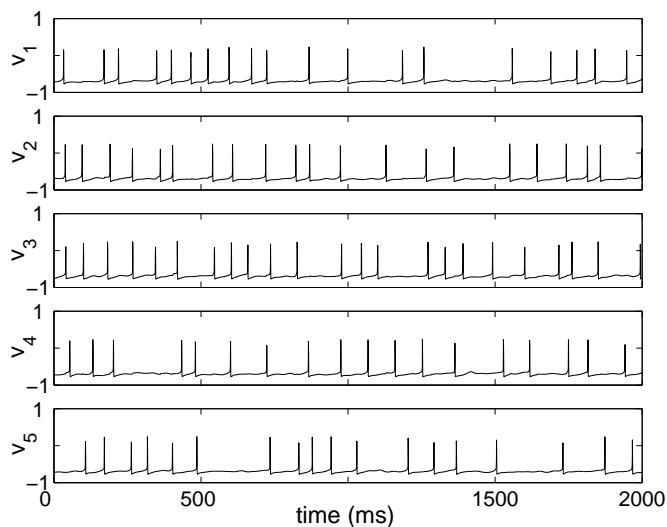


FIGURE 7. Simulated action potentials from five neurons in the Hodgkin-Huxley network model for $k = 2$.

portion of the total coupling energy (less than 5% in this example), we find that the result actually agrees with the original network architecture reasonably well.

Figure 8 indicates that the coupling strength measure C_{ji} can be used to estimate the network structure and the directions of interactions among neurons. Can it be used to assess the *changes* in interaction strength? Figure 9 shows how the coupling strength measure C_{ji} of each connection changes as the assumed coupling strength

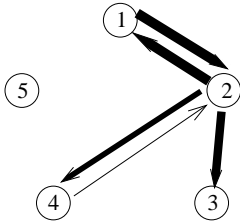


FIGURE 8. The estimated coupling architecture of the network with significant interactions, where 100 trials with $k = 2$ and the significance level $\alpha = 0.05$ are used. The arrows indicate the directions of coupling and the thickness of lines signifies the relative coupling strength.

k is increased from 1 to 4. For each value of k , 100 independent trials are used for estimating C_{ji} . Apparently, the estimated coupling strength reflects these changes. While C_{ji} gives the strength of individual connections, the summation of C_{ji} , ΣC , gives the estimation of the coupling-strength level of the whole network. Figure 10 shows that ΣC increases with k , indicating that our procedure can detect correctly the change in neural interactions.

3.2. Analysis of neural recordings from M1 during adaptation. In all trials of an experimental session (typically lasting for about one day), the same population of active neurons (about 30~50) are recorded simultaneously. A total of 44 M1 neurons are considered for this study. For each target, the number of trials is between 20 and 80. Our interest lies in how the neural interactions evolve during adaptation. Let Day 1 denote the first day of perturbed trials, or the first day of adaptation. That is, on Day 0, monkeys have already been well trained on unperturbed reaching-out movements. At the beginning of the perturbed trials, a monkey's reaching-out movement tends to be delayed significantly. However, after one week's training on perturbed trials, the monkey appears to have learned how to compensate for the perturbation and can finish the movement in a time about the same as that for the unperturbed trials, indicating that adaptation has taken place, which is also suggested by Figure 2. The typical patterns of changes in firing rates of individual neurons are shown in Figure 11, which was obtained from the responses toward target 4. It also appears that the changing patterns from different targets are similar for the same neuron during the adaptation. Among the 44 neurons, the firing rates of about 36% (16/44) of neurons were found to be fairly constant during pre-adaptation days, while the ones of the others were not. During the adaptation, the firing rates of about 18% (8/44) of neurons were found to have increased; 30% (14/44) increased first and then returned to their original values; 11% (5/44) decreased; 11% (5/44) decreased, increased, and then returned to their original values; 27% (12/44) showed no clear trend.

Figure 12 shows the average number of spikes during one trial. There are apparently large variations in the firing rate for different targets. In addition, some neurons appear to be very active (for example, firing more than 10 spikes in one trial), while others are not. For statistical reliability, we select 17 active neurons and group them into three sets for the purpose of cross validation. The first set consists of eight neurons that fire actively through the experiments on all the days.

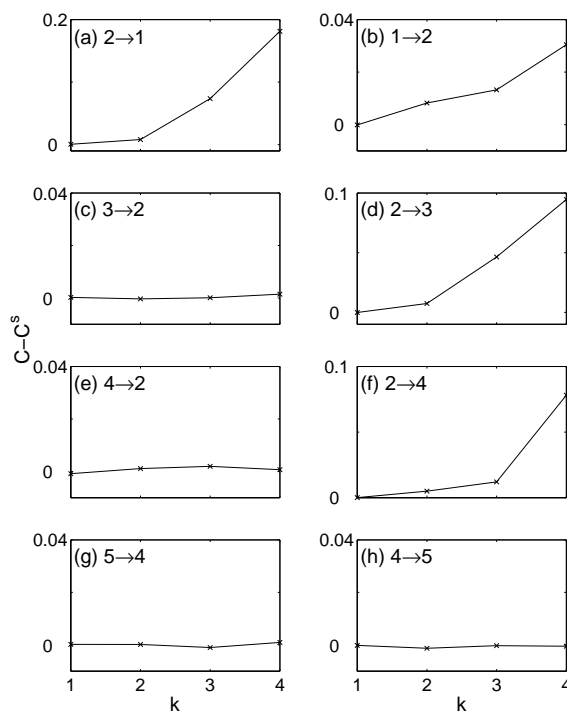


FIGURE 9. Estimated coupling strength of individual connections versus the assumed coupling strength k . Specifically, there is a mutual interaction between neurons 1 and 2, so the estimated values of $C_{12} - C_{12}^s$ and $C_{21} - C_{21}^s$ tend to increase as k is increased. The interaction between neurons 2 and 3 is unidirectional ($2 \rightarrow 3$), so the estimated coupling $C_{32} - C_{32}^s$ increases with k , but $C_{23} - C_{23}^s$ remains near zero, and so on. Neuron 5 is isolated, so there is no appreciable change from zero in its coupling with other neurons, as expected.

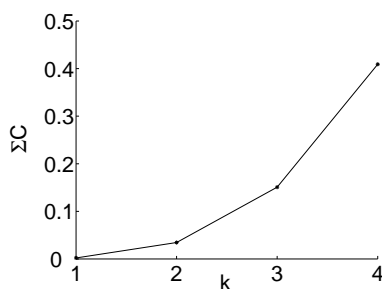


FIGURE 10. The estimated coupling-strength level averaged over the entire network, ΣC , versus the assumed coupling k .

The second set consists of six neurons (four are also in the first set), which also

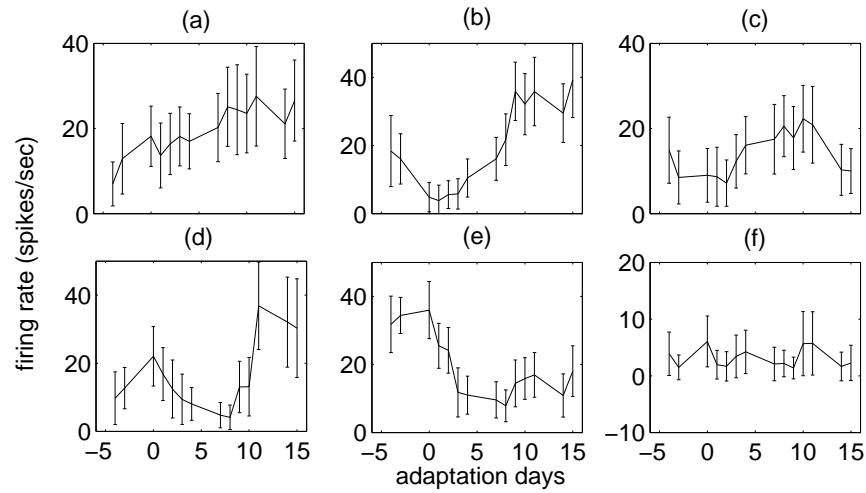


FIGURE 11. The changes of firing rates from six typical neurons in M1 across adaptation days. The firing rates are averaged over trials on target 4 during the time period from target-on to center-release.

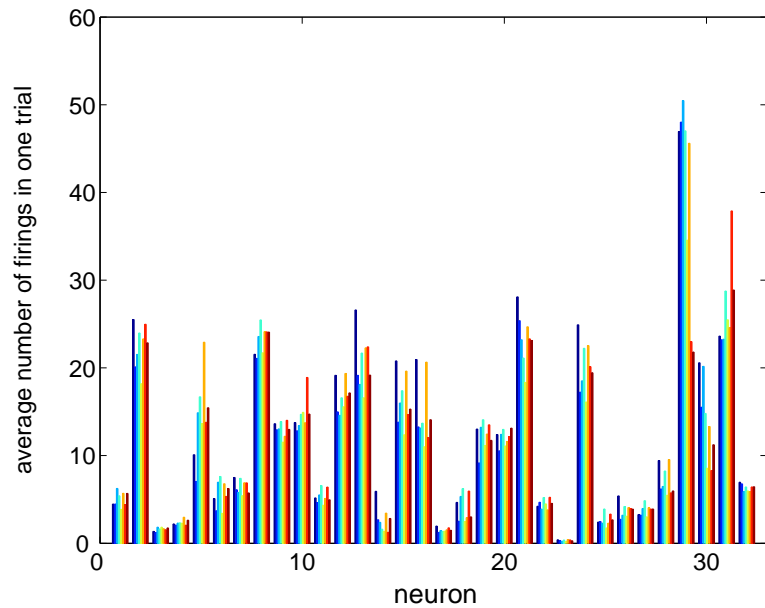


FIGURE 12. The average number of spikes during one trial on Day 0. There are 32 neurons actively firing on this day. The eight bars for each neuron correspond to eight targets.

fire actively throughout the experimental period. The third set varies on different days and consists of eight neurons that fire most actively on each day. For

each set on each day, the recorded spike trains are first preprocessed. The resulting data are then used to construct an MVAR model, and the coupling matrices are computed. Null hypothesis tests are performed to find statistically significant connections based on the empirical distributions obtained from the surrogate data.

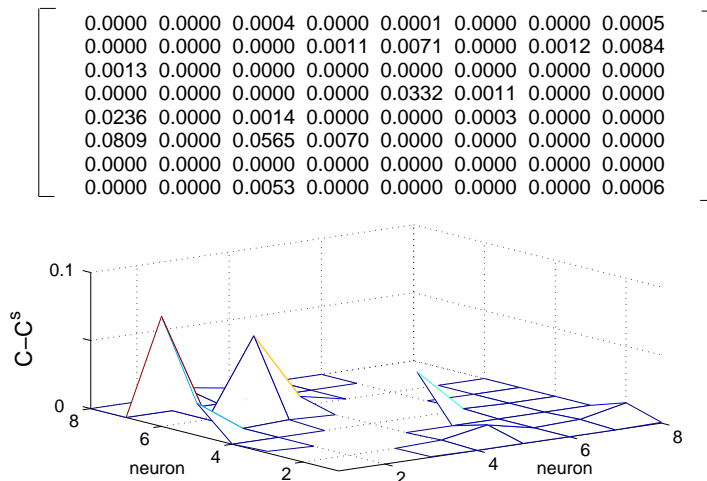


FIGURE 13. Interactions among eight neurons in motor cortex. Upper panel: The estimated coupling-strength matrix, where C^s is from surrogate data. The diagonal elements are excluded. If $C_{ij} < C_{ij}^s$, then it is replaced by zero. Lower panel: Graphic representation of the matrix $C - C^s$.

Figure 13 shows the estimation of typical interactions between eight neurons in M1, where (a) lists the 8×8 coupling matrix, and (b) is a graphic representation of the coupling matrix, excluding the diagonal elements. The peaks in (b) indicate relatively strong interactions among the corresponding neurons. The changes of interactions between some arbitrarily selected pairs of neurons in Set 1 during adaptation are shown in Figure 14 (a~h) (trials for target 7) and in Figure 15 (a~h) (trials for target 8). These observations provide direct evidence that adaptation is accompanied by synaptic change, which may occur rather quickly. These observations also support the suggestion that M1 is the site for memorizing motor skills, and learning can result in the build-up of an internal neural network in M1. A question is then whether the synaptic modification during adaptation tends to modify only slightly the connecting architecture of the neural network established during the learning process in unperturbed trials or to change the architecture totally (*i.e.*, reorganization of the interaction paths). Figures 14 (j~l) (trials for target 7) and 15 (j~l) (trials for target 8) show the architectures of the eight-neuron network on three days. We see that on the time scale of days, adaptation tends to change the interacting architecture within the network in a substantial manner, suggesting that the internal network of neurons in M1 is very flexible. Probably the strategy employed by the brain for adaptation in response to external perturbations is to reorganize the neural network. Results on other sets of neurons also support this observation (e.g., Set 2 on trials with target 4, as shown in Figure 16). Here we have investigated only a very small set of neurons, while learning and adaptation

in general may involve many neurons in M1 and in other regions of the brain as well. However, the neurons from which spike trains are recorded are randomly selected, so the 17 active neurons used in our analysis may constitute a reasonable representation of the entire population of the involved neurons in M1. We thus expect our observation of the change of the architecture of the neural network to be meaningful.

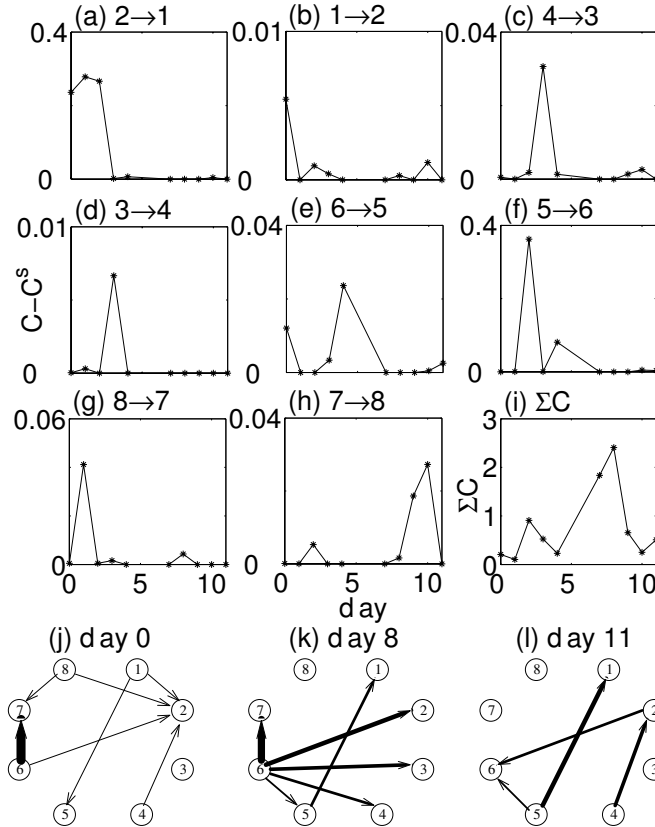


FIGURE 14. For trials with target 7. The eight most active neurons (Set 1) are investigated. (a~h) The estimated changes in coupling strength of individual connection during adaptation. The connections shown here are arbitrarily selected. (i) The changes in coupling-strength level of this eight-neuron network during adaptation. (j~l) Estimated network architecture for Days 0, 7 and 11 respectively, where the arrows indicate the directions of coupling and the thickness of lines signifies the relative coupling strength.

The overall changes of interaction level of the eight neurons in Set 1 for targets 7 and 8 are shown in Figures. 14 (i) and 15 (i). The general observation is the following: Although the directions and the coupling strength of neural interactions can change during the adaptation (as shown in Figures 14, 15, 16), the overall coupling level after the adaptation returns to the same level as before the adaptation. Results with other targets and more neurons, as shown in Figure 17, indicate

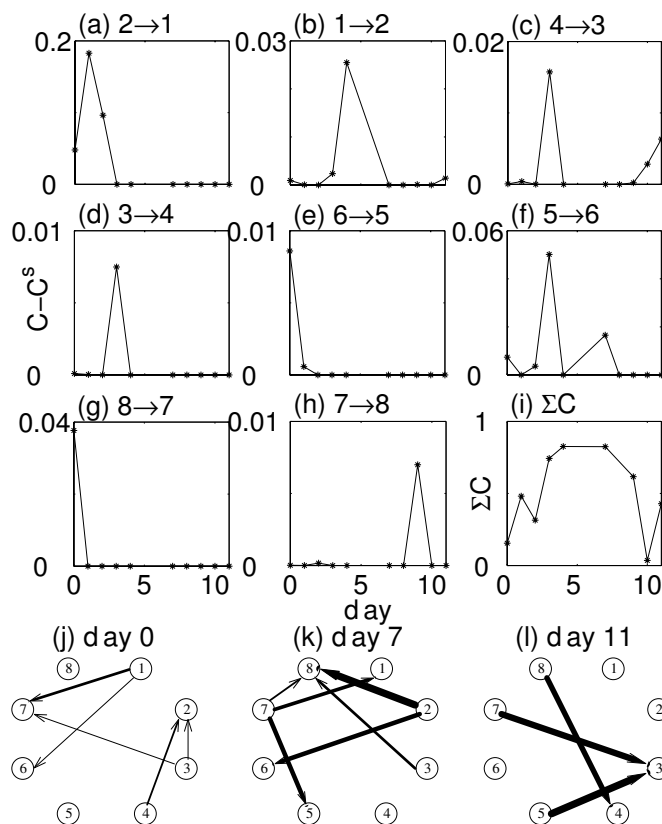


FIGURE 15. Results of neurons in Set 1 from trials with target 8. (a~l) The same as in Figure 14 except (k), which is for Day 8.

that the restoration of the coupling strengths after adaption appears to be the rule governing the change in neural interactions during adaptation.

4. Discussion. In this study, we have analyzed spike trains generated by M1 neurons from a monkey during reaching-out movements in a controlled environment. Once the skill has been learned, physical perturbations are applied to the monkey's arms during the movements so that its brain has to make adjustment to adapt to the perturbations. At first, the monkey's movements are shaky and delayed, but after a few days during which adaptation takes place, it can perform almost the movement as quickly as before. These processes of learning and adaptation tend to cause changes in the neural network in two ways.

First, during adaptation the synaptic strengths (or the coupling strengths) among neurons change and thus new dynamics take over in the network of neurons. Our analysis, based on a multivariate time-series technique, can reveal these synaptic strength changes in a direct way, indicating that the neurons in M1 take part in the establishment of the new dynamics. At the beginning of adaptation, the interactions among neurons tend to be strengthened. The result of stronger coupling strength among the neurons in a network is a way to have faster response to input stimulus for the whole network. That is, the increased coupling strength enables

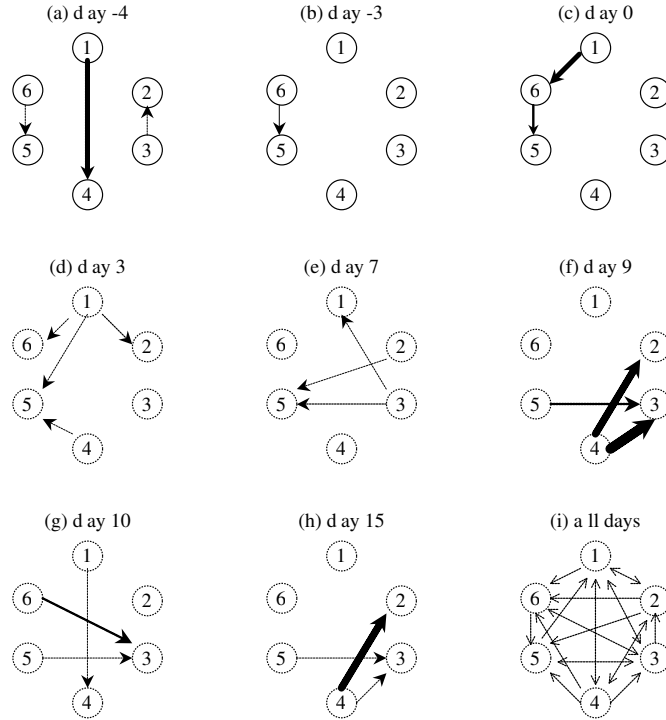


FIGURE 16. Results obtained from a set of six neurons (Set 2) on trials with target 4. (a~h) Estimated network structure on different days. The thickness of lines signifies the relative coupling strength. (i) All possible connections (regardless of their strengths) among these six neurons by superposing the results from 14 different days.

the monkey to respond to the external perturbation more quickly. The expense, however, is more energy consumption due to the increased coupling. Continuous training can still slightly improve the performance of the reaching-out movement. After adaptation, the overall coupling strengths among neurons return to the original level, which means less energy consumption for performing the task.

Second, our analysis reveals that the connecting architecture of the neural network tends to change significantly as a result of adaptation. Perhaps, to achieve fast response, changing the architecture may be better than increasing the coupling strength. For instance, Lago-Fernández et al. showed [42] that a few long-range, short-cut type connections can produce significantly faster response and coherent oscillations in the network. We can imagine that, at the beginning of the adaptation, after failure of several rounds of trials, the monkey must concentrate more on its arm's movement. (After the learning period, this movement may become a routine.) This attention shift results in stronger coupling strength. During a successful adaptation, the brain learns not only to adjust the synaptic weight but more important, to establish some long-range synapses. Initially the long-range

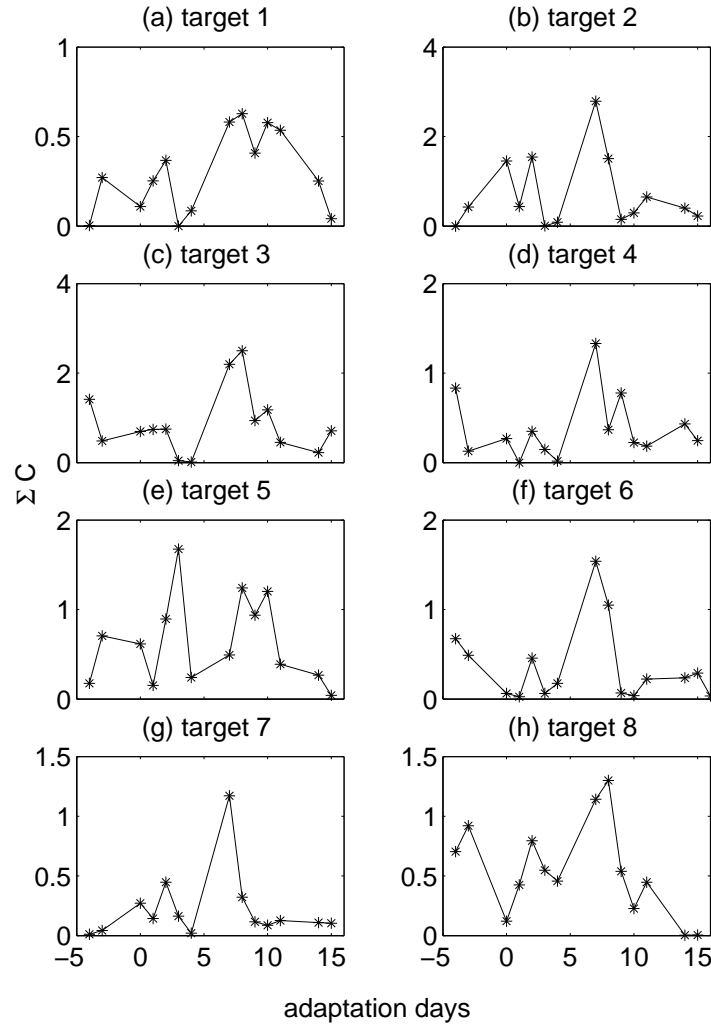


FIGURE 17. Estimated coupling-strength level across adaptation days. Results are obtained from 17 neurons.

weights may be weak, but they can become stronger, which is analogous to the case where short-cut type connections are created so that better performance is achieved [42]. It is possible that this learning process never stops, and over-training can always change the interactions among neurons. The above observation also indicates that good performance and energy efficiency are goals of the adaptation. While good performance was enforced by food rewards to the monkey, energy efficiency is achieved by the nature of the learning mechanism of the brain.

Acknowledgment. This work was sponsored by DARPA under Grant No. MDA972-00-1-0027.

REFERENCES

- [1] K. G. Pearson, NEURAL ADAPTATION IN THE GENERATION OF RHYTHMIC BEHAVIOR. *Annu. Rev. Physiol.* 62 (2000) 723~753.
- [2] M. Ito, MECHANISMS OF MOTOR LEARNING IN THE CEREBELLUM. *Brain Res.* 886 (2000) 237~245.
- [3] J. N. Sanes and J. P. Donoghue, PLASTICITY AND PRIMARY MOTOR CORTEX. *Annu. Rev. Neurosci.* 23 (2000) 393~415.
- [4] C.-S. R. Li, C. Padoa-Schioppa, and E. Bizzi, NEURONAL CORRELATES OF MOTOR PERFORMANCE AND MOTOR LEARNING IN THE PRIMARY MOTOR CORTEX OF MONKEYS ADAPTING TO AN EXTERNAL FORCE FIELD. *Neuron* 30 (2001) 593~607.
- [5] J. R. Muller, A. B. Metha, J. Krauskopf, and P. Lennie, RAPID ADAPTATION IN VISUAL CORTEX TO THE STRUCTURE OF IMAGES. *Science* 287 (1999) 1405~1408.
- [6] G. H. Recanzone, C. E. Schreiner, and M. M. Merzenich, PLASTICITY IN THE FREQUENCY REPRESENTATION OF PRIMARY AUDITORY CORTEX FOLLOWING DISCRIMINATION TRAINING IN ADULT OWL MONKEYS. *J. Neurosci.* 13 (1993) 87~103.
- [7] S. L. Florence and J. H. Kaas, LARGE-SCALE REORGANIZATION AT MULTIPLE LEVELS OF THE SOMATOSENSORY PATHWAY FOLLOWS THERAPEUTIC AMPUTATION OF THE HAND IN MONKEYS. *J. Neurosci.* 15 (1995) 8083~8095.
- [8] A. Karni, G. Meyer, P. Jezzard, M. M. Adams, R. Turner, and L. G. Ungerleider, FUNCTIONAL MRI EVIDENCE FOR ADLT MOTOR CORTEX PLASTICITY DURING MOTOR SKILL LEARNING. *Nature* 377 (1995) 155~158.
- [9] R. J. Nudo, G. W. Milliken, W. M. Jenkins, and M. M. Merzenich, USE-DEPENDENT ALTERATIONS OF MOVEMENT REPRESENTATIONS IN PRIMARY MOTOR CORTEX OF ADULT SQUIRREL MONKEYS. *J. Neurosci.* 16 (1996) 785~807.
- [10] P. M. Gochin, E. K. Miller, C. G. Gross, and G. L. Gerstein, FUNCTIONAL INTERACTIONS AMONG NEURONS IN INFERIOR TEMPORAL CORTEX OF THE AWAKE MACAQUE. *Exp. Brain Res.* 84 (1991) 505~516.
- [11] R. B. Duckrow and S. S. Spencer, REGIONAL COHERENCE AND THE TRANSFER OF ICTAL ACTIVITY DURING SEIZURE ONSET IN THE MEDIAL TEMPORAL LOBE. *Electro. Clin. Neurophysiol.* 82 (1992) 415~422.
- [12] S. L. Bressler, R. Coppola, and R. Nakamura, EPISODIC MULTIREGIONAL CORTICAL COHERENCE AT MULTIPLE FREQUENCIES DURING VISUAL TASK PERFORMANCE. *Nature* 366 (1993) 153~156.
- [13] S. Grün, M. Diesmann, and A. Aertsen, UNITARY EVENTS IN MULTIPLE SINGLE-NEURON SPIKING ACTIVITY: II. NONSTATIONARY DATA. *Neural Comput.* 14 (2002) 81~119.
- [14] R. Güttig, A. Aertsen, and S. Rotter, STATISTICAL SIGNIFICANCE OF COINCIDENT SPIKES: COUNT-BASED VERSUS RATE-BASED STATISTICS. *Neural Comput.* 14 (2002) 121~153.
- [15] G. Pipa and S. Grün, NON-PARAMETRIC SIGNIFICANCE ESTIMATION OF JOINT-SPIKE EVENTS BY SHUFFLING AND RESAMPLING. *Neurocomputing* 52 (2003) 31~37.
- [16] P. Whittle, ON THE FITTING OF MULTIVARIATE AUTOREGRESSIONS AND THE APPROXIMATE FACTORIZATION OF A SPECTRAL MATRIX. *Biometrika* 50 (1963) 129~134.
- [17] W. Gersch, SPECTRAL ANALYSIS OF EEG'S BY AUTOREGRESSIVE DECOMPOSITION OF TIME SERIES. *Math Biosci.* 7 (1970) 205~222.
- [18] M. Ding, S. L. Bressler, W. Yang, and H. Liang, SHORT-WINDOW SPECTRAL ANALYSIS OF CORTICAL EVENT-RELATED POTENTIALS BY ADAPTIVE MULTIVARIATE AUTOREGRESSIVE MODELING: DATA PREPROCESSING, MODEL VALIDATION, AND VARIABILITY ASSESSMENT. *Bio. Cybern.* 83 (2000) 35~45.
- [19] M. J. Kaminski and K. J. Blinowska, A NEW METHOD OF THE DESCRIPTION OF THE INFORMATION FLOW IN THE BRAIN STRUCTURES. *Biol. Cybern.* 65 (1991) 203~210.
- [20] K. Sameshima and L. A. Baccala, USING PARTIAL DIRECTED COHERENCE TO DESCRIBE NEURONAL ENSEMBLE INTERACTIONS. *J. Neurosci. Methods* 94 (1999) 93~103.
- [21] W. A. Freiwald, P. Valdes, J. Bosch, R. Biscay, J. C. Jimenez, L. M. Rodriguez, V. Rodriguez, A. K. Kreiter, and W. Singer, TESTING NON-LINEARITY AND DIRECTEDNESS OF INTERACTIONS BETWEEN NEURAL GROUPS IN THE MACAQUE INFEROTEMPORAL CORTEX. *J. Neurosci. Methods* 94 (1999) 105~119.
- [22] M. Kaminski, M. Ding, W. A. Truccolo, and S. L. Bressler, EVALUATING CAUSAL RELATIONS IN NEURAL SYSTEMS: GRANGER CAUSALITY, DIRECTED TRANSFER FUNCTION AND STATISTICAL ASSESSMENT OF SIGNIFICANCE. *Bio. Cybern.* 85 (2001) 145~157.

- [23] C. W. J. Granger, INVESTIGATING CAUSAL RELATIONS BY ECONOMETRIC MODELS AND CROSS-SPECTRAL METHODS. *Econometrica* 37 (1969) 424~438.
- [24] L. Zhu, Y.-C. Lai, F. C. Hoppensteadt, and J. He, PROBING CHANGES IN NEURAL INTERACTION DURING ADAPTATION. *Neural Computation* 15 (2003) 2359~2377.
- [25] F. Takens, in *Dynamical Systems and Turbulence*, edited by D.A. Rand and L.-S. Young, Lecture Notes in Mathematics 898 (Springer-Verlag, Berlin, 1981) 366~381.
- [26] T. Sauer, J. A. Yorke, and M. Casdagli, EMBEDDING. *J. Stat. Phys.* 65 (1991) 579~616.
- [27] H. Kantz and T. Schreiber, *NONLINEAR TIME SERIES ANALYSIS*. Cambridge University Press, Cambridge, UK, 1997.
- [28] T. Sauer, RECONSTRUCTION OF DYNAMICAL SYSTEMS FROM INTERSPIKE INTERVALS. *Phys. Rev. Lett.* 72 (1994) 3811~3814.
- [29] T. Sauer, INTERSPIKE INTERVAL EMBEDDING OF CHAOTIC SIGNALS. *Chaos* 5 (1995) 127~132.
- [30] R. Castro and T. Sauer, CORRELATION DIMENSION OF ATTRACTORS THROUGH INTERSPIKE INTERVALS. *Phys. Rev. E* 55 (1997) 287~290.
- [31] D. J. Weber, CHRONIC, MULTI-ELECTRODE RECORDINGS OF CORTICAL ACTIVITY DURING ADAPTATION TO REPEATED PERTURBATIONS OF REACHING. Ph.D. Dissertation, Dept. of Bioengineering, Arizona State University, 2001.
- [32] H. Akaike, A NEW LOOK AT THE STATISTICAL MODEL IDENTIFICATION. *IEEE Trans. Auto. Control* 19 (1974) 716~723.
- [33] W. J. Freeman, MODELLING THE EEG WITH NONLINEAR DYNAMICS. *Electroen. Clin. Neuro.* 61 (1985) S224.
- [34] W. J. Freeman and C. A. Skarda, SPATIAL EEG PATTERNS, NONLINEAR DYNAMICS AND PERCEPTION - THE NEO-SHERRINGTONIAN VIEW. *Brain Res. Rev.* 10 (1985) 147~175.
- [35] W. J. Freeman, BRAINS MAKE CHAOS TO MAKE SENSE OF THE WORLD. *Behav. Brain Sci.* 10 (1987) 161~173.
- [36] Y.-C. Lai, I. Osorio, M. A. F. Harrison, and M. Frei, CORRELATION-DIMENSION AND AUTOCORRELATION FLUCTUATIONS IN EPILEPTIC SEIZURE DYNAMICS. *Phys. Rev. E* 65 (2002) 031921 (1~5).
- [37] J. Theiler, S. Eubank, A. Longtin, B. Galdrikian, and J. D. Farmer, TESTING FOR NONLINEARITY IN TIME SERIES: THE METHOD OF SURROGATE DATA. *Physica D* 58 (1992) 77~94.
- [38] D. R. Brillinger, COMPARATIVE ASPECTS OF THE STUDY OF ORDINARY TIME SERIES AND POINT PROCESSES. *Developments in Statistics* 5 (1978) 33~133.
- [39] F. Rieke, D. Warland, R. Van Steveninck, and W. Bialek, *SPIKES : EXPLORING THE NEURAL CODE*. MIT Press, Cambridge, MA, 1997.
- [40] A. Riehle, S. Grün, M. Diesmann, and A. Aertsen, SPIKE SYNCHRONIZATION AND RATE MODULATION DIFFERENTIALLY INVOLVED IN MOTOR CORTICAL FUNCTION. *Science* 278 (1997) 1950~1953.
- [41] H. R. Wilson, *SPIKES, DECISIONS, AND ACTIONS: THE DYNAMICAL FOUNDATIONS OF NEUROSCIENCE*. Oxford University Press, Oxford, 1999.
- [42] L. F. Lago-Fernández, R. Huerta, F. Corbacho, and J. A. Sigüenza, FAST RESPONSE AND TEMPORAL COHERENT OSCILLATIONS IN SMALL-WORLD NETWORKS. *Phys. Rev. Lett.* 84 (2000) 2758~2761.

Received on Aug. 17, 2004. Revised on Oct. 15, 2004.

E-mail address: lqzhu@asu.edu

E-mail address: Ying-Cheng.Lai@asu.edu

E-mail address: Jiping.He@asu.edu

E-mail address: fh21@nyu.edu